Monatshefte für Chemie 130, 961–982 (1999)

Monatshefte für Chemie
Chemical Monthly

Printed in Austria

Invited Review

NMR Techniques to Study Hydrogen Bonding in Aqueous Solution[a]

Robert Konrat*, **Martin Tollinger, Georg Kontaxis**[b], and **Bernhard Kräutler**

Institute of Organic Chemistry, University of Innsbruck, Austria

Summary. Recent improvements in NMR methodology have significantly increased the scope of hydrogen bond related problems that can be now addressed by solution NMR methods. A growing number of applications are exploiting these NMR techniques to study complex molecular systems and elicit otherwise inaccessible information on hydrogen bonding in aqueous solution.

Keywords: Hydrogen bond; NMR Spectroscopy; Chemical shift anisotropy; Isotopic fractionation factor; Hydrogen exchange.

NMR-Spektroskopie von Wasserstoffbrücken in wäßriger Lösung

Zusammenfassung. Kürzlich erarbeitete methodische Weiterentwicklungen der Kernresonanzspektroskopie erlauben nunmehr auch Untersuchungen von Wasserstoffbrücken in wäßriger Lösung. Diese neuartigen experimentellen Methoden wurden bereits erfolgreich angewandt, um geometrische und energetische Wasserstoffbrückenparameter in Lösung zu bestimmen.

Introduction

The hydrogen bond [1–5] is considered to be not only a significant determinant of the solution structure of biomolecules, but also of crucial importance to all biochemical processes by contributing to transition state stabilization or to ligand binding specificity. Hydrogen bonds also control chemical self-assembly processes by which 'programmed' molecular subunits spontaneously form complex supramolecular frameworks [6, 7]. The hydrogen bond A-H$\cdots B$ is typically described as an electrostatic attraction between the positive end of the bond dipole of A-H and a centre of negative charge on B [4]. In a typical situation, A is sufficiently electronegative to ensure a strongly polar bond. The acceptor site on B is typically

* Corresponding author

[a] Dedicated to Prof. *H. Gruber* on the occasion of his 70th birthday

[b] Present address: Laboratory of Chemical Physics, National Institute of Diabetes and Digestive and Kidney Diseases, National Institute of Health, Bethesda, Maryland, USA

defined as a lone pair. Thus, the hydrogen bond inherently involves the sharing of hydrogen atoms to varying extents with other atoms, typically leading to a lengthening of the donor H-bond and shortening overall the distance to acceptor *B*. It is generally assumed that the hydrogen bond is a weak interatomic interaction, and that it is an order of magnitude weaker than covalent bonding. However, there are cases (*e.g.* charged species in the gas phase) where the strength of hydrogen bonds are comparable to those of covalent bonds. Ionization greatly affects hydrogen bonding. If the donor is positively charged $(A\text{-H})^+$, there will be an increased electrostatic attraction between the donor and the acceptor *B*. By the same token, a negatively charged acceptor *B* will strengthen the hydrogen bonding.

Bond lengths, energetics, vibrational frequencies, electron distributions, and various other spectroscopic characteristics are modified upon formation of a hydrogen bond. The structural characteristics of hydrogen bonds (*e.g.* hydrogen bond lengths, proton location, bond angles) are studied by X-ray or neutron diffraction techniques. Based on X-ray studies, a correlation was established between the distances $R_{A\text{-}B}$ and $R_{A\text{-H}}$. The most notable observation is the decrease in $R_{A\text{-}B}$ accompanied by an increase in $R_{A\text{-H}}$ [3, 4]. This relationship also serves to classify hydrogen bonds. Typically, weak bonds are characterized by $R_{A\text{-}B} > 260$ pm, the hydrogen essentially staying close to its directly attached atom [3]. Strong hydrogen bonds show $R_{A\text{-}B}$ values in the range of 245–260 pm. In this case, the proton tends to move from the donor atom *A* towards the acceptor atom *B* [3]. Finally, very strong hydrogen bonds have $R_{A\text{-}B} < 245$ pm, and the proton is located roughly halfway between the two heteroatoms [3].

Experimental information on hydrogen bond energies are available from measurements either in the gas phase [3, 8, 9] or under nonaqueous conditions [10–13]. From measurements by ion cyclotron resonance spectroscopy [3], the energies of a broad range of hydrogen bonds could be determined with values up to and exceeding $84\ \text{kJ} \cdot \text{mol}^{-1}$ (in charge localized and ionic species in the gas phase) [3], depending on the length of the hydrogen bond and the distance between the hydrogen bond donor and acceptor atoms. Empirically it was found that as a hydrogen bond becomes shorter it becomes stronger. For example, $(H_2O)_2$ has a $R_{O\text{-}O}$ distance of 297 pm and a hydrogen bond energy *E*(OHO) of about $21.7\ \text{kJ} \cdot \text{mol}^{-1}$ [3]. In contrast, 3-(4′-biphenyl)pentane-2,4-dione has a $R_{O\text{–}O}$ distance of 244 pm and a *E*(OHO) of about $117\ \text{kJ} \cdot \text{mol}^{-1}$ [3]. Electrostatic attraction accounts for the energies of weak hydrogen bonds. When a molecule forms a hydrogen bond, the vibrational modes are considerably changed and can be monitored using either IR or *Raman* spectroscopy where the stretching vibration of the donor bond, $\nu(A\text{H})$, decreases in frequency. In certain cases, the shift can amount to hundreds of wavenumbers, and this change has been related to hydrogen bond energies (Ref. [3] and references cited therein).

In this review we will focus on and limit the discussion to NMR based techniques to characterize hydrogen bonding. Starting from already established spectroscopic manifestations such as characteristic downfield shifts of the proton resonances [3] or the isotope fractionation factor φ [3], we will discuss intermolecular exchange rate measurements (k_{ex}) of exchangeable protons and introduce solution measurements of the chemical shift anisotropy (CSA) of hydrogen as sensitive probes for hydrogen bonding in aqueous solution.

Chemical Shift and Chemical Shift Anisotropy

As a rule, hydrogen bonding leads to a downfield shift of the NMR resonance of the hydrogen bonded hydrogen [3]. Solid state NMR revealed a qualitative correlation between the hydrogen bond length and the downfield shift of the isotropic chemical shifts (σ_{iso}) of the hydrogen bonded hydrogens [3]. There is an extensive literature about correlations between the easily accessible spectral parameter σ_{iso} and other hydrogen bond related parameters, *e.g.* hydrogen bond distances, variations in the ν_{AH} stretching frequencies, linear stretching force constant, and quadrupolar coupling constant (e^2qQ/h). In liquids, the proton chemical shift can be used to calculate thermodynamic parameters associated with hydrogen bonding [3].

The two nearby nuclei in the hydrogen bond *A*-H···*B* cause the ^{1}H NMR signal of *A*-H···*B* to occur further downfield than the resonance of a similar proton A-*H* that cannot form a hydrogen bond [3]. This deshielding effect was explained by *ab initio* calculations on hydrogen bonded O-H···O systems [14, 15]. The deshielding of the isotropic chemical shift was explained by three effects. First, the proton loses electron density upon hydrogen bond formation, and due to the fact that there are only *s* functions on the hydrogen, the chemical shift tensor components are deshielded isotropically. In addition, the acceptor oxygen deshields the perpendicular components but shields the parallel component. Third, the oxygen atom of the hydrogen bond donor accounts for some deshielding in the perpendicular components and can either shield or deshield the parallel component. In sum, this leads to a net deshielding of both the isotropic chemical shift and the perpendicular components of the chemical shift tensor. Multiple pulse NMR experiments of *e.g.* O-H···O systems in the solid state [16] confirmed the predicted correlation between the isotropic chemical shift σ_{iso} and the O···O separation $R_{O\cdots O}$. In this study, a maximum downfield shift of about 10 ppm for σ_{iso} was found. The σ_{iso} value was suggested to be the preferable NMR probe for hydrogen bonding, as it is least sensitive to extraneous effects (*e.g.* nearby ions or atoms in the solid state environment). However, measurements of the individual tensor components revealed a more detailed picture of the effect of hydrogen bonding geometry (*e.g.* $R_{O\cdots O}$) on spectral parameters. It was found, that the perpendicular components of the chemical shift tensor, $\sigma_\perp$, are very sensitive to $R_{O\cdots O}$, whereas the parallel component $\sigma_\parallel$ is almost unchanged. A significant correlation between $\sigma_\perp$ and the quadrupolar coupling constant e^2qQ/h was also observed, and since e^2qQ/h correlates very well to the hydrogen bond strength, $\sigma_\perp$ is largely responsible for the observed changes in σ_{iso} and in the chemical shift anisotropy (CSA) $\Delta\sigma = \sigma_\parallel - \sigma_\perp$ as the degree of hydrogen bonding changes.

Upon hydrogen bond formation involving (protein) amide protons H^N, a similar redistribution of electron density takes place resulting in a more polar charge distribution (*e.g.* favouring the more polar resonance structures). The direction of the electron density shift from the NH to the carbonyl group results in a decreased magnetic shielding for the amide proton and hence results in a shift to lower field of its ^{1}H NMR signal. This downfield shift of the isotropic amide proton signal is accompanied by an increase in chemical shift anisotropy (CSA) upon hydrogen bond formation. In peptidic systems, there exist only three solid-state NMR studies

of backbone amide H^N CSA values [17–19]. All data indicate that, although the H^N CSA tensor can deviate from axial symmetry, the most shielded tensor component is aligned along the N–H bond. Recently, the magnitudes and orientations of the principal elements of the ^{1}H chemical shift interaction tensor of the NH side-chain protons of ^{15}N-labeled tryptophan and histidine residues were also determined [20]. Hence, ^{1}H chemical shift anisotropy $\Delta\sigma = \sigma_{\parallel} - \sigma_{\perp}$ should be a very sensitive indicator for hydrogen bonding also in solution. It should be noted that hydrogen bonding can also be studied using heteronuclear NMR spectroscopy, as heteroatoms also change their spectroscopic properties upon hydrogen bonding. For example, in case of peptides or proteins, it is an important question to define hydrogen bond donors and hydrogen bond acceptors. Solid-state NMR experiments on peptides have delineated the effects which govern the chemical shifts of carbonyl carbons, amide nitrogens, and amide protons as a function of the hydrogen bonding capabilities of different solvents [21–23]. It was found that carbonyl protonation (*e.g.* carbonyl oxygen is the hydrogen bond acceptor) causes a deshielding of the amide nitrogen [22] similar to that of the amide proton [23]. The situation was found to be more complex for the carbonyl carbon NMR chemical shift [21]. Although a low field shift of the peptide carbonyl resonance results from carbonyl protonation (H bond acceptor role), H bonding of the covalently linked NH group (H bond donor role) leads to an increased shielding of the carbonyl carbon atom. Hence, the opposite chemical shift trends caused by either NH or C=O hydrogen bonding can sometimes cancel each other and thus render the hydrogen bonding of the peptide group undetectable by chemical shift arguments. From a comparison of calculated and experimental ^{15}N chemical shift tensors of benzamide, it was concluded that chemical shift anisotropy is a very sensitive probe for hydrogen bonding [24], as the variation of the individual tensor components could be masked by measurements of the traditional isotropic chemical shift value σ_{iso}, which is defined as the trace of the chemical shift tensor.

Another very sensitive spectral probe for studying hydrogen bond properties in solution is the heteronuclear scalar coupling constant (*e.g.* $^1J_{NH}$). Because a one-bond spin coupling is a through-bond phenomenon, it is a direct measure of the covalent bond character (*e.g.* hybridization, bond length). For example, *Limbach* and co-workers have used $^1J_{NH}$ couplings to monitor a gradual intermolecular proton transfer between ^{15}N-pyridine and *o*-tolylic acid or 2-thiophenecarboxylic acid [25]. The $^1J_{NH}$ coupling constants increased from almost 0 to about 90 Hz upon proton displacement. *Bachovchin* and co-workers [26] have used $^1J_{NH}$ coupling constants (amongst other experimental parameters) to provide experimental evidence against the existence and catalytical importance of a putative low-barrier hydrogen bond (LBHB) in serine proteases. They measured the imidazole N–H spin coupling constants for protonated His^{57} and neutral His^{57} in the catalytic triad Asp^{102}-His^{57}-Ser^{195}. From the experimental values of 80±4 Hz for protonated His^{57} and 90±1 Hz for neutral His^{57}, they concluded that the the proton is essentially localized on $N^{\delta 1}$ in neutral His^{57} and at least 85% on $N^{\delta 1}$ when His^{57} becomes protonated and engaged in the putative LBHB. The estimation was based on the one-bond coupling constant $^1J_{HF} \approx 120$ Hz for the bifluoride ion (FHF^-) in dipolar aprotic solvents. The coupling is about one-forth of that observed for HF (476 Hz) [27]. The decrease in the $^1J_{HF}$ coupling constant in (FHF^-) very nicely

demonstrates the sensitivity of this NMR parameter. Recently, protein-solvent hydrogen bonding was studied by $^1J_{NC'}$ coupling constants [28]. It was demonstrated that $^1J_{NC'}$ significantly increases ($^1J_{NC'} > 17$ Hz) upon hydrogen bond formation between the carbonyl oxygen and water molecules at that site, whereas extremely low values ($^1J_{NC'} < 14$ Hz) correspond to the absence of hydrogen bonds at the respective carbonyl sites.

Rapid tumbling motion of a molecule in solution causes an averaging of the tensorial interaction between the chemical shift tensor of a particular spin and the external magnetic field [29]. The anisotropy of the chemical shift tensor, observed as an orientational dependence of the chemical shift tensor in the solid (powder pattern) [30] is not manifested in high resolution NMR spectra in solution, but is reduced to the isotropic chemical shift, σ_{iso}. Chemical shift anisotropy (CSA), however, is responsible for an important relaxation mechanism of spin systems in solution and has been the subject of detailed investigations since the early ages of NMR [31–33]. Although experimental studies have dealt mostly with ^{19}F, ^{13}C, and ^{31}P nuclei, it is now well established that even protons can have significant and detectable CSA contributions to their relaxation [34–37]. Relaxation interference effects (*e.g.* cross-correlations), as was first pinpointed by *McConnell* [38], between CSA and dipolar couplings contain information on motional properties and chemical shift tensors. These cross-correlated relaxation mechanisms lead to a conversion of *e.g.* longitudinal *Zeeman* order $\langle \boldsymbol{I}_{zk} \rangle$ into longitudinal two-spin order and $\langle 2\boldsymbol{I}_{zk}\boldsymbol{I}_{zl} \rangle$ [33] and can effectively be monitored by double-quantum filtered correlation spectroscopy (DQF-COSY) [36]. It also gives rise to unusual line shapes (*e.g.* differential line broadening) [33]. The effect of differential line broadening is not limited to single-quantum coherence (SQC), but a general phenomena of nuclear coherences [39], and defines the basis for a new group of pulse sequences to determine protein backbone dihedral angles [40, 41]. Specifically, in a weakly coupled AX spin system, the decay rate of the low-field component of the doublets will be faster than the decay of the upfield components, the difference being given by

$$(1/T_2)^{\beta} - (1/T_2)^{\alpha} = 16/3\, J_{AXA}(0) + 4J_{AXA}(\omega_A) \tag{1}$$

For isotropic molecular motion, the cross-correlation spectral density function $J_{AXA}(\omega_A)$ is given by the following expression:

$$J_{AXA}(\omega_A) = 1/10(\mu_0/4\pi)\gamma_A^2\gamma_X h\langle \boldsymbol{r}_{AX}^{-3} \rangle B_0 \Delta\sigma_A(\tau_c/(1+\omega_A^2\tau_c^2))1/2(3\cos^2\varphi_{AXA} - 1) \tag{2}$$

where B_0 is the strength of the magnetic field, $\Delta\sigma_A$ the chemical shift anisotropy of proton A, and φ_{AXA} the angle between the unique axis of the CSA tensor σ_A and the internuclear vector $\boldsymbol{r}_{AX}$. The CSA tensor is assumed to be axially symmetric in these equations; more general expressions have been given [33]. The cross-correlation rate $J_{AXA}(\omega_A)$ can simply be determined by monitoring the individual decay rates of the two doublet components. For ^{15}N-enriched biomolecules, more elaborate experimental schemes have been proposed [42–44]. They are based on either conversion of in-phase coherence (transverse one-spin order) into anti-phase magnetization (transverse two-spin order), or on measurements of the relative

amplitudes of the two doublet components at the end of a constant-time evolution period. As was reported for O-H···O hydrogen bonds [16], the HN proton CSA also depends strongly on the length of the hydrogen bond. For example, the measured values found in the protein ubiquitin ($MW = 8.6$ kD) ranged from near zero in the absence of hydrogen bonding to about 14 ppm for residues involved in short hydrogen bonds. Most important, an increase in hydrogen bond strength increased the shielding parallel to the N–H bond but decreased the shielding orthogonal to this bond. As a consequence, hydrogen bonding is more sensitively probed by CSA than by measurements of the istropic chemical shift σ_{iso}. A dependence of CSA on secondary structure was observed. α-Helical amide protons have smaller CSA values (7.2 ± 1.5 ppm) in contrast to solvent exposed amide protons (10.5 ± 1.6 ppm) and amide protons located in β-sheets (11.2 ± 1.6 ppm) [42].

Experimental aspects

In recent NMR-spectroscopic and structural studies [45–47] of the B_{12}-cofactor methylcobalamin (**1**) in aqueous solution, several conformational differences between the solution structure and the crystal structure [48] of **1** were observed, notably in the nucleotide loop. Conformational information obtained from ROESY data together with dihedral angle constraints obtained from three-bond homo- and heteronuclear scalar coupling constants and the spectral observation of the solvent exchangeable *R*2′-OH hydroxyl proton allowed the identification of an internally bound water molecule, linking the polar phosphate group, the amide group (N174), and the *R*2′-OH of the ribose moiety of the nucleotide loop [47]. The bound water molecule thus acts as the responsible restructuring element for the nucleotide loop of methylcobalamin in aqueous solution (Fig. 1). This detection of an exchange-labile OH-hydrogen in aqueous solution is remarkable, as precedence for such a situation is scarce [49–51]. It indicates the labile *R*2′-OH hydrogen of the ribose unit of **1** to be involved in a (*pseudo*)intramolecular hydrogen bond and to be protected in this way from exchange with the solvent. Figure 2 shows a ^{1}H NMR spectrum of methylcobalamin [45] dissolved in 90%H_2O/10%D_2O. Due to solvent presaturation, the *R*2′-OH hydroxyl ribose proton signal was barely observed at 5.5 ppm. Selective excitation resolved the signal as a doublet with 4.5 Hz splitting (Fig. 3). Up to now, only a few $^3J_{(HOCH)}$ coupling constants have been reported, and a *Karplus* relationship for a similar system is not available in the literature. The observed coupling constant of 4.5 Hz for $^3J_{(HOCH)}$ allows for an additional dihedral angle constraint with respect to the spatial orientation of the *R*2′-OH hydroxyl group consistent with a structure in which O–H points roughly towards H(N174) and suggests a *gauche* conformation (*ca*. 60°) rather than an angle close to the *Karplus* maxima (180° or 0°) or near the *Karplus* minimum (90°). The decay rates of the two doublet components of the hydroxyl hydrogen *R*2′-OH in methylcobalamin were determined by a standard *Carr-Purcell-Meiboom-Gill* (CPMG) T_2-pulse sequence [52], but using multiplet selective excitation [53] and inversion pulses [54] (see legend of Fig. 3). Figure 3 shows the decay of the two doublet components. From the differential decay of the two doublet components, the cross correlation rate was determined to be about 1.1 Hz using Eq. (1). The

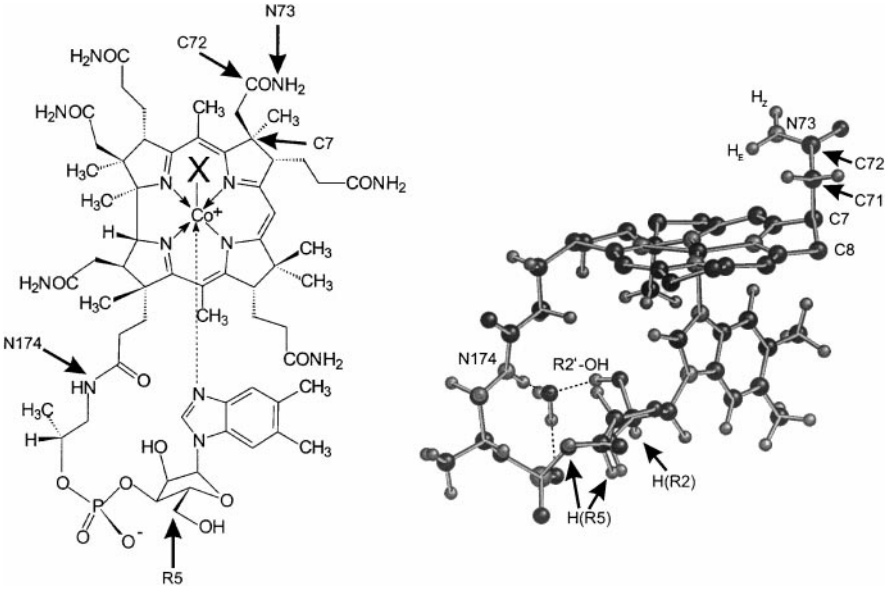

Fig. 1. (Left) Structural formula of methylcobalamin (**1**, $X = CH_3$) and the aquocobalamin cation (**2**, $X = H_2O^+$); (Right) View of relevant parts of the solution structure of **1**, showing the corrin macrocycle, the nucleotide loop, and the c-acetamide side chain, highlighting the internal, tetrahedrally coordinated water, the hydroxyl hydrogen *R*2′-OH, and the amide proton H(N174). The dashed lines represent hydrogen bonds

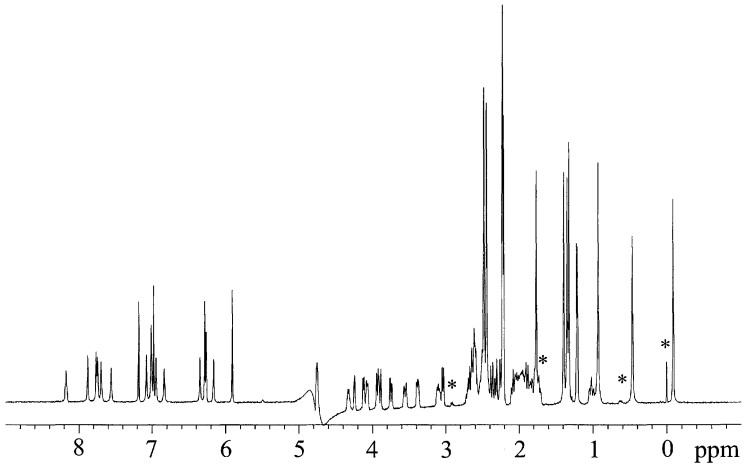

Fig. 2. 500 MHz ^{1}H NMR spectrum of **1** dissolved in 90% H_2O/10% D_2O

chemical shift anisotropy $\Delta\sigma_A$ was calculated to be about 28 ppm from Eq. (2) (assuming axial symmetry of the magnetic shielding tensor) and taking the dihedral angle φ_{AXA} and the distance r_{AX} from the solution structure of methylcobalamin where A is *R*2′-OH and X is H(*R*2), respectively. The overall reorientational correlation time τ_c was determined to 250 ps based on ^{13}C-T_1 values determined by standard inversion-recovery experiments. This proton CSA value is very close to

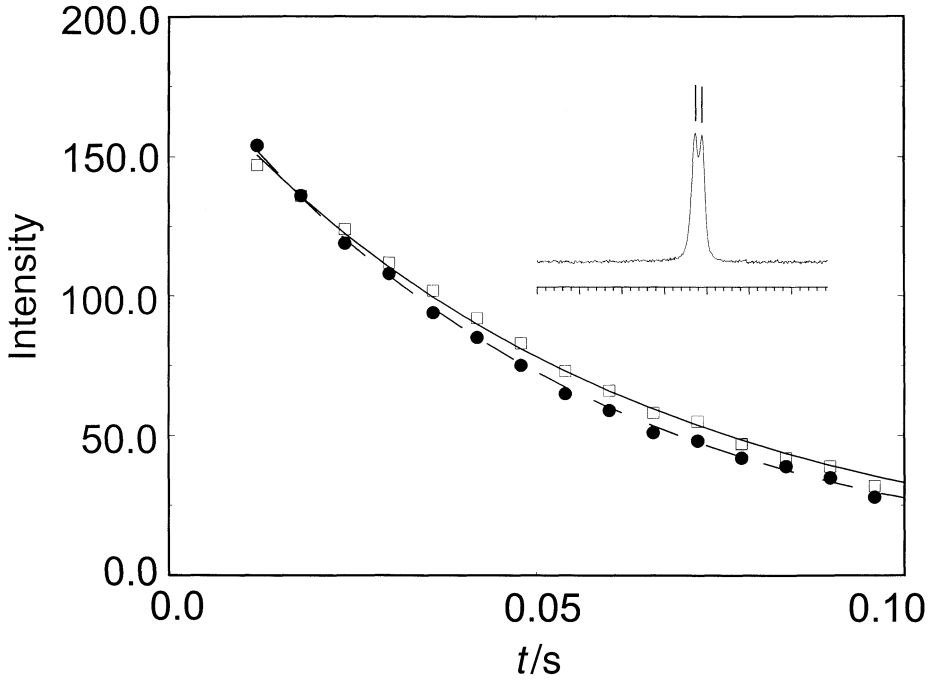

Fig. 3. T_2-decay curves for the doublet components of $R2'$-OH in methylcobalamin. Selective T_2-measurements were performed using a 30 ms 270° *Gaussian* excitation pulse [53] and 50 ms G3 *Gaussian* cascade inversion [54] RF pulses. From the differential decay of the two doublet components, a chemical shift anisotropy - dipolar cross correlation rate (CSA-DD) of 1.1 Hz was determined. Using Eq. (2), the chemical shift anisotropy of the $R2'$-OH proton was calculated to $\Delta\sigma = 28$ ppm (see text)

values obtained from proton anisotropic chemical shift spectra obtained in a single crystal of hexagonal ice (28.5 ppm) [55] and proton NMR powder spectra of ice, 34.2±1.0 [56] and 34±4 ppm [57]. Theoretical calculations studying the influence of secondary hydrogen-bonding effects on the shielding of hydrogens in ice also confirmed both a CSA value of about 30 ppm and the axial symmetry of the magnetic shielding tensor of a hydroxyl proton involved in a hydrogen bond [58]. Thus, the hydrogen bond formed between the $R2'$-OH and the internal, tetrahedrally coordinated water molecule is well defined in solution and comparable to hydrogen bonds formed between water molecules in the solid state.

H/D Isotope Fractionation Factor

The isotopic fractionation factor φ of an exchange-labile proton in a molecule is defined as the equilibrium constant for the exchange process of this particular proton with deuterons from the solvent:

$$X\mathrm{H} + \mathrm{D}S(\text{bulk solvent}) \rightleftharpoons X\mathrm{D} + \mathrm{H}S(\text{bulk solvent})$$

$$\varphi = \frac{[X\mathrm{D}][\mathrm{H}S]}{[X\mathrm{H}][\mathrm{D}S]}$$

A value of 1 reflects an equal distribution of protons and deuterons between the exchange-labile position *X* and the solvent *S*; a φ value >1 indicates a preference for D over H on the position *X*, whereas a value <1 indicates a preference for H over D. The equilibrium constant can be analyzed in terms of relative zero-point energies of the *X*-H and *X*-D bonds [3, 59–61]. Fractionation factors can be rationalized qualitatively by considering effective one-dimensional potentials or effective force constants. In case that the exchange-labile site *X* has a stronger force constant for the bond *X*-[H, D] than for the solvent *S*, the fractionation factor will be >1 and *vice versa*. In the case of a hydrogen bond *X*-H$\cdots$*Y*, the force constant of the *X*-H bond is decreased resulting in a fractionation factor < 1. There is extensive literature about deuterium fractionation factors for low molecular weight compounds such as alcohols, phenols, carboxylates, hydroxyls, imidazoles, amines, and amides, most of them being close to 1 in aqueous solution [62–64]. Deviations occur for hydrogen bonded systems. For example, in weakly bound solute-solvent complexes of water-dioxane, water-methanol, and tetrahydrofuran-fluoroform, fractionation factors > 1 have been observed. In contrast, compounds that form strong hydrogen bonds typically exhibit low fractionation factors ($\varphi < 1$), *e.g.* F_2H^- in water ($\varphi = 0.6$), dimers of 4-nitrophenolate ($\varphi = 0.31$), trifluoroacetate ($\varphi = 0.42$), 3,5-dinitrobenzoate ($\varphi = 0.30$), 3,5-dinitrophenolate ($\varphi = 0.36$), and pentachlorobenzoate ($\varphi = 0.40$) (all in acetonitrile) [65]. The larger values of φ in protic solvents is presumably due to competing hydrogen bonding with the solvent. Until recently, spectral complexity confined the measurements of isotopic fractionation factors to low molecular weight compounds. Exceptions were measurements on *e.g.* the hydrogen shared between the two glutamate residues E168 and E211 in enolase and that between glutamate E217 and N1 of bound adenosine in adenosine deaminase, each having φ values of about 0.4 [66–68]. In this case, the particular low φ values have been attributed to low-barrier hydrogen bonds, and the importance of this type of hydrogen bonding to enzyme catalysis has been discussed by *Cleland* [66]. Recently, a new NMR method was introduced [69, 70] which allows for the determination of fractionation factors in uniformly ^{15}N-labeled proteins. The method relies on measurement of the intensities of ^{15}N-^{1}H correlations in a range of H_2O/D_2O solvent mixtures. This technique has been applied to staphylococcal nuclease both in its unligated state and in its ternary complex with Ca^{2+} and the inhibitor thymidine 3′,5′-bisphosphate [70]. The fractionation factors varied between 0.34 (threonine T120) and 1.42 (glycine G55), with average values and standard deviations of 0.84 ± 0.19 and 0.86 ± 0.17 for unligated and ligated nuclease. α-Helical regions displayed values of about 0.79 ± 0.10, whereas slightly larger φ-values (0.91 ± 0.15) were found for residues located in β-sheet secondary structures. No clear correlation was found between fractionation factors and N–O distances for the amide-amide hydrogen bonds observed in the crystal structure of unligated nuclease. This reflects the subtle interplay of mechanisms responsible for determining fractionation factor in complex molecules (*e.g.* off-line bending motions in addition to in-line stretching vibrational oscillations around the equilibrium position). Additionally, conformational differences between the solid and the liquid state of staphylococcal nuclease could not be ruled out. However, the significantly reduced value ($\varphi = 0.34$) for the backbone amide of threonine T120 was attributed to a hydrogen bond formed with

the charged side-chain carboxylate group of aspartate D77. Thus, in accordance with data obtained in the gas-phase, hydrogen bonds involving a charged acceptor site were found to be energetically more favourable and displayed decreased fractionation factors. In general, the study showed that, on average, protium is accumulated to the greatest extent in α-helices and at sites of cooperative hydrogen bonds involving charged moieties, in contrast to the enrichment of deuterium seen in more unstructured parts of the proteins (*e.g.* loop regions).

Experimental aspects

Although fractionation factors φ can be obtained from the resonance intensities (*i.e.*, the protium level) in a single spectrum of known intermediate solvent composition (for example 50% D_2O), it is more accurate to determine the proton occupancies at a particular molecular site as a function of solvent composition. Fractionation factors can be obtained by linear least-squares analysis of

$$1/y = C(\varphi(1-x)/x + 1) \tag{3}$$

where y is the peak area (intensity), x is the mole fraction of H_2O, and C is a normalization factor [70]. Of course, it is crucial that equilibrium has been reached before spectra are acquired. If there is no spectral overlap, one-dimensional ^1H NMR spectra are sufficient to obtain the necessary information. To obtain absolute intensities as a function of solvent composition, the signals can either be referenced to an external or internal standard (*e.g.* other non-exchangeable protons of the molecule). We have recorded ^1H spectra of methylcobalamin (**1**) (see Figs. 1 and 2) at different solvent composition, and the signal intensities of *R*2′-OH as a function of H_2O mole fraction is shown in Fig. 4. The fractionation factor for

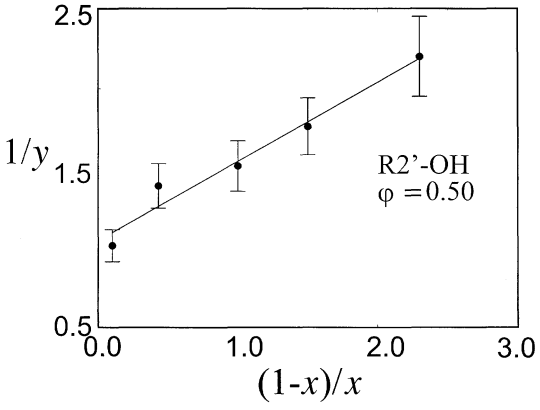

Fig. 4. Measurement of H/D fractionation of *R*2′-OH in methylcobalamin. Plots of normalized ^1H NMR signal intensity (yC) as a function of the mole fraction H_2O (x) according to the equation [69,70] $(yC)^{-1} = (\varphi(1\text{-}x)/x)+1$, where y is the signal intensity, C is a normalization factor, and the slope of the line is the H/D fractionation factor (φ). The signal intensity y was obtained by referencing to the non-exchangeable methyl proton signal which resonates most upfield in the ^1H NMR spectrum (0.5 ppm). To minimize signal attenuation of the exchanging *R*2′-OH signal due to exchange with bulk water, selective excitation of the *R*2′-OH signal (50 ms, self-compensating *Gaussian* excitation pulse [53]) was applied

*R*2′-OH was determined to be 0.5 (according to Eq. (3)), typical for an exchangeable proton involved in a strong hydrogen bond, and corroborates the existence of the hydrogen bond formed to the internally coordinated water molecule as delineated from NOEs and coupling constant information (see below).

The dimensionality of the experiment and thus the spectral resolution can be increased by recording a ^{1}H-^{15}N correlation spectrum [69, 70], or, if a doubly labeled protein is available, a HA(CA)CO spectrum [71]. In this experiment, the $^{1}H^{\alpha}$ resonance of residue *i* is correlated with the intraresidue carbonyl $^{13}C'$ resonance. If the sample is equilibrated in 50% H_2O/50% D_2O, the $^{1}H^{\alpha}$-$^{13}C'$ correlation will show a splitting in the $^{13}C'$ dimension as a result of the two-bond isotope shift, corresponding to protonated and deuterated states of the directly attached nitrogen. Thus, there is no need for external referencing, and very accurate data can be obtained on a sample dissolved in a solvent mixture of 50% H_2O/50% D_2O. However, if no isotope labeling is available or if rapidly exchanging and hence unresolved hydroxyl protons (rapidly exchanging protons experience a chemical shift similar to bulk water) are under scrutiny, we have devised an alternative method to study fractionation factors in aqueous solution. The experimental scheme is basically a 2D ROESY [72] sequence with standard modifications to ensure water suppression using pulsed field gradients according to the WATERGATE technique [73]. In the 2D ROESY experiment, cross peaks are found at the water chemical shift in the indirect dimension and non-exchangeable protons H_{non} in the direct dimension. This transfer is caused by a relay mechanism [74] which depends on the nature of magnetization transfer operative during the spin lock period, consisting of both TOCSY-type transfer due to scalar coupling (^{n}J(OH-H_{non})) [74] and dipolar interaction (σ_{ROE}). The flow of magnetization for this process is as follows:

$$\boldsymbol{I}_x(H_2O) \rightarrow (k_{ex}) \rightarrow \boldsymbol{I}_x(OH) \rightarrow {}^{n}J(OH - H_{non})/\sigma_{ROE} \rightarrow H_{non} \qquad (4)$$

The intensities of these exchange-relayed cross peaks are governed by the transfer function (scalar and/or dipolar coupling) and the spin densities of the protons involved. The transfer function and the spin densities of the non-exchangeable protons do not change with solvent composition. In contrast, the spin densities of exchangeable protons (*e.g.* hydroxyl protons) are a function of the H_2O/D_2O ratio. Hence, measuring cross peak intensities for a range of H_2O/D_2O solvent mixtures gives an estimate of the spin densities of the exchangeable protons or, in other words, the H/D isotope fractionation factor φ. We have again used the corrinoid cofactor methylcobalamin (**1**) as an example. A recent NMR study has shown that the solution structure is considerably different from the crystal state, mainly caused by the existence of an internal tetrahedrally coordinated water molecule. The hydrogen bonding network of this water molecule comprised the secondary ribose hydroxyl hydrogen (*R*2′-OH), which significantly retarded the intermolecular exchange with bulk water and allowed the NMR observation of this hydroxyl hydrogen at 5.50 ppm. The hydrogen of the primary ribose hydroxyl group (*R*5′-OH) was still unobservable due to rapid exchange. Figure 5 shows a trace taken from a 2D ROESY spectrum of methylcobalamine along the water resonance in ω_1. Apart from negative cross peaks which are due to intermolecular ROEs between hydration water molecules and protons of methylcobalamin, there are four

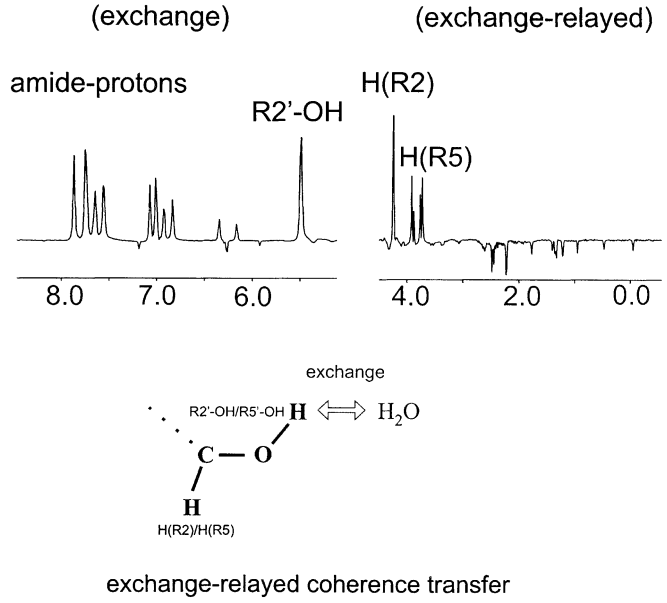

Fig. 5. Cross section parallel to the ω_2-axis taken at the ω_1 frequency of the water resonance through a 200 ms WATERGATE-ROESY of methylcobalamin (**1**). Water NOEs found for protons located near the bulk water hydrations sites occur as negative cross peaks in the spectrum. Positive cross peaks belong to exchange cross peaks with the bulk water signal (*R*2′-OH at 5.50 ppm) or exchange-relayed cross peaks (H(*R*2), H(*R*5a), H(*R*5b)), typical of protons located in the vicinity of exchangeable protons [74]

interesting positive cross peaks: *R*2′-OH, H(*R*2), and the two diastereotopic protons H(*R*5a) and H(*R*5b). The cross peak between bulk water and *R*2′-OH is caused by intermolecular exchange, whereas the others are exchange-relayed peaks, presumably due to TOCSY-type transfer. For the determination of φ, the general procedure of *Loh* and *Markley* was used [69, 70]. Four samples with varying amounts of H_2O/D_2O were prepared; the mole fractions (x) of H_2O were 0.9, 0.7, 0.5, and 0.3. The spin densities of the exchangeable protons were determined by measuring the relative ROESY cross peak intensities between a pair of non-exchangeable protons and a cross peak involving the exchangeable proton of interest (see legend of Fig. 6). Figure 6 shows a linearized plot of the intensities *vs.* H_2O mole fraction according to Eq. (3). Due to the resolved resonance of *R*2′-OH, both, direct ROESY cross peaks between *R*2′-OH and non-exchangeable protons (H(*R*2)) as well as exchange-relayed cross peaks (detected at H(*R*2) at the bulk water trace in ω_1) could be analyzed. Quantitative interpretation of the measured spin densities as a function of solvent composition was achieved by calibration with one-dimensional ^{1}H-spectra (see above). This was necessary because the absolute values of the experimentally determined spin densities are additionally governed by magnetization exchange between the solvent and the solute, a process which itself is a function of the deuteration level. For example, solvent presaturation and/or the use of an interscan delay shorter than the long solvent T_1 attenuates resonances of protons in rapid exchange with solvent. Direct and

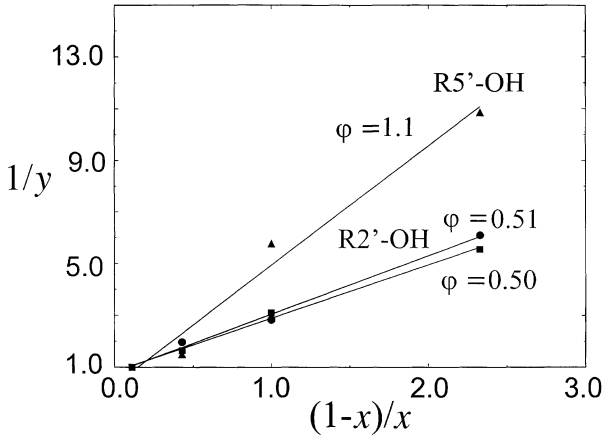

Fig. 6. Measurement of H/D fractionation of *R*2′-OH in methylcobalamin based on a two-dimensional ROESY experiment. Plots of normalized cross peak intensity (*yC*) as a function of the mole fraction H_2O (*x*) according to Refs. [69,70]. The signal intensities *y* for *R*2′-OH were obtained from referencing the direct (exchange, shown as squares) bulk water ROESY cross peak of *R*2′-OH to ROESY cross peaks of *R*2′-OH to non-exchangeable protons H(*R*2). A second set of data for *R*2′-OH was obtained using the exchange-relayed cross peak of H(*R*2), as taken from the water trace (Fig. 5) and again referencing to a cross peak involving a non-exchangeable proton (shown as circles). The H/D fractionation of *R*5′-OH was determined only from the exchange-relayed cross peak to both H(*R*5) protons

exchange-relayed magnetization transfer results in identical values for φ, thus proving the reliability of the method (Fig. 6). The φ values for *R*2′-OH obtained with the three methods discussed were 0.50 (one-dimensional ^{1}H-based method, reference value; Fig. 4), 0.50 (direct transfer), and 0.51 (exchange-relayed transfer). The significantly reduced value of φ is due to hydrogen bond formation to the internally bound water molecule. For the rapidly exchanging *R*5′-OH proton a fractionation factor of about 1.1 was obtained using the relayed magnetization transfer. This is expected for exchangeable protons which are not involved in strong hydrogen bonds. In solution, the *R*5′-OH of methylcobalamine points towards the solvent and is freely accessible to bulk water molecules. Similar values were found for low molecular weight alcohols and hydroxyls in aqueous solution [62–64]. This shows that even for rapidly exchanging hydroxyl protons the 2D ROESY experiment provides unique access to φ values which otherwise cannot be obtained in aqueous solution.

Intermolecular XH Exchange

Hydrogens bound to N, O, and S atoms of polar groups within a solute molecule dissolved in water are in continual exchange with the hydrogens of the solvent. In contrast, carbon-bound hydrogens do not exchange easily. Although polar-group hydrogens (*X*H) are generally exchange-labile, they are covalently bound and exchange with solvent hydrogens only as a result of distinct chemical reactions. The underlying catalytic reaction steps are reversible proton transfer reactions

between donor and acceptor groups. The primary step in a proton transfer reaction can be regarded as a diffusion-limited collision and hydrogen bond formation between a proton donor (*A*H) and a proton acceptor (*B*), leading to a so-called encounter complex. The next event is a proton redistribution across the hydrogen bond, apparently *via* quantum mechanical tunneling [76].

$$AH + B \underset{k_{-D}}{\overset{k_D}{\rightleftharpoons}} (AH\text{---}B \overset{K_C}{\rightleftharpoons} A\text{---}HB) \underset{k_D}{\overset{k_{-D}}{\rightleftharpoons}} A + HB$$

The equilibrium constant for this reversible proton redistribution is given by

$$K_c = 10^{\Delta pK} \tag{5}$$

where

$$\Delta pK = pK_B - pK_A \tag{6}$$

For a successful proton transfer reaction, the reaction rate k_{tr} is given by

$$k_{tr} = k_D(10^{\Delta pK}/10^{\Delta pK} + 1) \tag{7}$$

where k_D is the second order rate constant for the diffusion-limited collision. Hence, the rate-limiting step for a hydrogen exchange reaction is the proton transfer reaction from the proton donor (acid) to the proton acceptor (base). Thus, k_{ch}, the intrinsic chemical exchange rate characteristic of the catalyst (*Cat*), can be set equal to the limiting proton transfer rate constant k_{tr} (Eq. (7)). In general, more than one catalyst can be present, and the resulting first order exchange rate constant (k_{ex}) is given as the sum of all possible contributions.

$$k_{ex} = \Sigma\, k_{ch}[Cat] \tag{8}$$

Two cases can be distinguished: the transfer of a proton proceeding either energetically downhill (from a stronger to a weaker acid, $\Delta pK > 1$) or uphill (from a weaker to a stronger acid, $\Delta pK < 1$). In the first case, every collision leads to a successfull proton transfer, and transfer proceeds at the maximum diffusion-limited rate defined by k_D. For example, nucleic acid NH ring protons or polar protein side chain protons (*e.g.* OH) have *pK*-values much lower than 15; therefore, exchange of these protons is very effectively catalyzed by the hydroxyl ion. Examples for the latter case are peptide amide protons. The deprotonation *pK* for a peptide group CONH is about 18.5 [76]. As a consequence, proton exchange of peptide amide groups is dominated by base catalysis down to about $pH = 3$. The first order exchange rate constant (k_{ex}) (assuming OH^- and H^+ being the only catalysts) is thus given by

$$k_{ex} = k_{OH}[OH^-] + k_H[H^+] \tag{9}$$

k_{OH} and k_H are defined according to Eq. (7). In the case of protein amides, this results in a V-shaped $\log(k_{ex})$ *vs. pH* profile with a minimum rate occurring between *pH* 2 and 3. This only holds for small molecules. In contrast, in more complex molecules (*e.g.* proteins, nucleic acids, protein complexes), a variety of factors can influence the exchange rates. Nearest neighbour groups can impose inductive (electron withdrawing) or electrostatic effects that shift the minimum of the *pH* profile along the *pH* axis. Steric effects can modify the accessibility and, hence, the

second order rate constant for the formation of the encounter complex. For peptide group amide protons, the important factors have been accurately calibrated in small molecule models [77–79]. Thus, it is now possible to reliably predict intermolecular exchange rates for random-coil polypeptides (and also polynucleotides) under ambient conditions. The most important influence imposed by the structure of the molecule, however is caused by a possible engagement of the exchangeable proton in a hydrogen bond. Proton transfer always requires, a an intermediate step, the formation of a hydrogen bond between donor and acceptor (exchange catalyst and, for example, protein amide proton). If the donor proton or the acceptor site is already involved in a pre-existing intramolecular hydrogen bond, the transfer will be impeded, and exchange significantly slowed down. This has already been reported in *Eigen's* classical work on proton transfer theory [80]: the hydroxylic proton of salicylate is removed by $^{-}$OH three orders of magnitude slower than the diffusion-limited rate, characteristic for non-hydrogen bonded hydroxyl protons. Many other examples exist which display slowing factors of up to almost six decades [81, 82] and demonstrate that significant hydrogen bonding can be found also in small molecules. Protein hydrogen exchange studies were initiated by *Linderstrøm-Lang* in the mid-1950s [83, 84] and have played a major role in the description of protein stability, protein folding and unfolding events, and in the characterization of the dynamical properties (*e.g.* structural fluctuations) of proteins ever since (for broad background reviews on this subject, see Refs. [60, 76, 85]). It is generally assumed that protection of amide protons in proteins from exchange with solvent protons involves hydrogen bonding. The exchange of protected protons occurs through structural fluctuations, leading to a transient severing of the blocking hydrogen bond. Exchange of the peptide amide proton with solvent protons can only occur in the open state, in which the hydrogen bond has been broken. In the closed state, the proton is still involved in the hydrogen bond and cannot form the rate-limiting hydrogen bond to the exchange catalyst. However, the open state can differ from the closed state by more than the hydrogen bond alone. As examples, neighbouring secondary structure segments may unfold in a cooperative manner or, alternatively, the open state can be differently stabilized by additional favourable interactions. Thus, the probability of the open state will depend not only on the free energy of the hydrogen bond but rather on both the hydrogen bonding energy of the closed (native) state and the interactions forming in the open state. The kinetic and thermodynamic relationships that relate structural isomerization (the breakage of a blocking hydrogen bond) with measured exchange rates (k_{ex}) were first formulated by *Berger* and *Linderstrøm-Lang* [86]. More general formulations have been given by *Hvidt* and *Nielsen* [60].

The observed exchange rate k_{ex} is given [76] by

$$k_{ex} = k_{op}k_{ch}[Cat]/(k_{cl} + k_{ch}[Cat]) \tag{10}$$

in which k_{op} and k_{cl} are the rate constants for the breakage and forming of the blocking hydrogen bond. k_{ch} is the intrinsic chemical exchange rate of the catalyst (*Cat*). Two cases can be distinguished. If refolding of the structural opening is fast compared to the intrinsic exchange rate ($k_{cl} \gg k_{ch}[Cat]$), exchange will be a second order reaction dependent on the concentration of the catalyst ($k_{ex} = K_{op}k_{ch}[Cat]$; $K_{op} = k_{op}/k_{cl}$). This limiting case is also known as the EX2 limit [76,87]. From the

value of K_{op} (determined by $K_{op} = k_{ex}/k_{ch}[Cat]$), the free energy stabilizing the closed (native) state can then be determined from the expression $\Delta G = -RT \ln K_{op}$. In contrast, the EX1 limit is reached when reforming of the hydrogen bond is slower than the intrinsic intermolecular exchange with solvent protons. The exchange rate is then equal to the opening rate k_{op} of the structural isomerization process (the breakage of the hydrogen bond).

Although a large number of different techniques for hydrogen exchange measurements exist [88–92], the ultimate resolution of measuring hydrogen exchange at individual atomic sites is only offered by neutron diffraction [93] and by NMR methods. In this review, we limit our discussion to NMR based methods. In principle, three fundamentally different NMR methods exist. Firstly, hydrogen exchange can be probed by so-called exchange-out techniques [88]. The intensity of the resonance line of a particular proton is proportional to the proton (^{1}H) concentration at this respective site. The time dependence of the line intensity after exposure to D_2O is a direct measure of the exchange rate at that particular site. If the signals are not separated, two-dimensional homonuclear or heteronuclear NMR experiments have to be applied. This type of experiments have successfully been applied to proteins and protein complexes [94–100]. A most striking application of this technique was the identification of an antibody binding site on Cytochrome c, defined by hydrogen exchange rates combined with the resolution obtained from a two-dimensional ^{15}N-^{1}H correlation spectrum [101]. Secondly, hydrogen exchange rates can be measured by saturation transfer techniques [102], where attenuation of the exchangeable proton signal is monitored after extended irradiation of the water signal. In its simplest form, the exchange rates of rapidly exchanging protons are measured from the effect of presaturation on simple one-dimensional spectra [103–105]. This requires the recording of two one-dimensional spectra in H_2O with and without presaturation of the water resonance. An extended version of the original experiment and applicable to ^{15}N-labeled proteins was introduced [106]. A third class of experiments is based on dynamic NMR spectroscopy [107]. Chemical exchange with bulk water protons contributes an additional relaxation mechanism to the transverse relaxation of the exchangeable proton. By measuring the transverse relaxation rate and accounting for non-exchange contributions, the exchange rate can be measured.

Experimental aspects

We have recently determined the crystal structure and the solution structure of aquocobalamin by NMR spectroscopy [108] (see Fig. 1). The NMR data confirmed the crystallographically determined occupation of the axial coordination site at the Co(III) center by water, as well as the occurrence of an intramolecular hydrogen bond to the axially coordinating water molecule in solution as observed in the crystal structure of the aquocobalamin ion. However, significant differences of the structure of aquocobalamin in the crystalline state and in aqueous solution were indicated from NOE data concerning the time-averaged conformation of the hydrogen bonding c-acetamide side chain ($H_{E/Z}N73$). The H-bonding c-acetamide side chain exhibits a *syn-clinal* arrangement of the bonds C8–C7 and C71–C72 (Fig. 1), whereas in the crystal structure these bonds are nearly *anti-periplanar*. In

the crystal structure of aquocobalamin, the (less basic) lone pair, oriented *trans* to the amide nitrogen, accepts the hydrogen bond. Hence, in solution the carbonyl oxygen lone pair oriented *cis* to the amide nitrogen is indicated to act as the hydrogen bond acceptor for the cobalt coordinated water proton in solution. We have investigated the chemical exchange behaviour of the amide proton H_E(N73) and could unambigiously demonstrate the engagement of this amide group in an intramolecular hydrogen bond to the cobalt coordinated water. Intermolecular exchange rates with bulk water protons were measured using a saturation transfer based NMR method [102–105]. To this end, we have recorded two sets of one-dimensional ^{1}H spectra (with and without presaturation of the water resonance) as a function of *pH*. In the absence of cross relaxation, attenuation of the amide resonance in the experiment with presaturation depends on the amide hydrogen exchange rate, k_{ex}, in the following manner [105]:

$$k_{ex} = (1 - M_{ps}/M_0)/T_{1app} \tag{11}$$

Here M_{ps} is the resonance intensity in the experiment with presaturation, M_0 is its intensity without presaturation, and T_{1app} is the apparent longitudinal relaxation rate as measured in a selective T_1 experiment. T_{1app} includes the effects of both exchange and true relaxation. Eq. (11) can be rewritten as

$$k_{ex} = (M_0/M_{ps} - 1)/T_1 \tag{12}$$

where T_1 describes the true longitudinal relaxation as measured in a selective T_1 experiment in the absence of chemical exchange. Typically, this rate is dominated by the cross-relaxation to other protons. For small compounds, homonuclear cross-relaxation is typically much smaller than the intrinsic longitudinal relaxation rate and therefore may be safely neglected. For proteins, however, the k_{ex} values as determined from Eq. (12) may include a substantial contribution from magnetization exchange caused by cross-relaxation. Examination of the *pH vs*. exchange rate profile (Fig. 7) for hydrogen exchange of amide protons with bulk water indicated the c-acetamide group H_E(N73) to exchange its protons slower at a *pH* smaller than *ca*. 3.5 but faster at a *pH* above about 3.5 than, for example, the acetamide function attached to the a-acetamide side chain H_E(N23). Thus, an increased resistance against acid catalyzed hydrogen exchange, as well as an increased rate of apparent base catalyzed hydrogen exchange, can be determined for the c-acetamide function. This apparent acidification of the c-acetamide function can be rationalized by the existence of a specific hydrogen bond involving its carbonyl oxygen. The existence of the H-bond between the cobalt-coordinated water molecule and the c-acetamide carbonyl oxygen is also supported by arguments based upon ^{15}N-chemical shifts (see above).

The application of dynamic NMR spectroscopy to studies of hydrogen bonding is exemplified by NMR investigations of the *R*2′-OH hydroxyl proton in methylcobalamin [45–47]. The measurement (see legend of Fig. 8) of T_2 relaxation and (from there) of the exchange rate k_{ex} of the 2′-OH hydrogen *via* NMR in the ribose moiety of methylcobalamin as a function of *pH* provided the intermolecular exchange profile shown in Fig. 8. The experimental data could be simulated with a non-linear least-squares fit according to Eq. (9). This result indicates the prevalence of the so-called EX2-limit [76, 87], implying that the

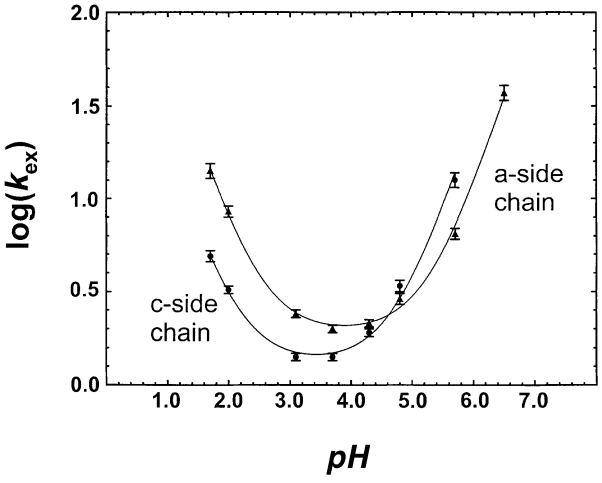

Fig. 7. Amide hydrogen bonding probed by intermolecular exchange measurements. *pH* profile of the intermolecular proton exchange rates (s^{-1}) of the trans (H_E) amide protons of the two acetamide (a, H_E(N23); c H_E(N73)) functions in aquocobalamin [107]. The experimental data for each acetamide were fitted by a hyperbola according to Eq. (9). Exchange rates were determined using saturation transfer [101] as described in the text

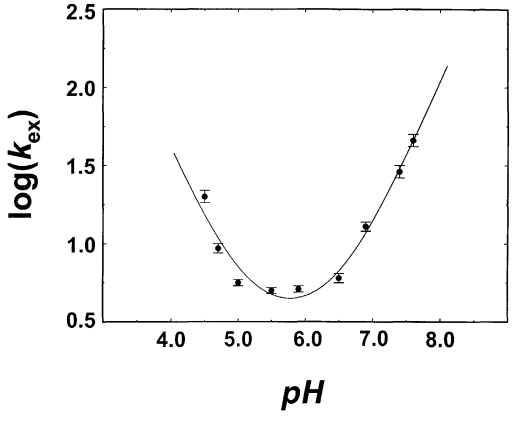

Fig. 8. Intermolecular exchange profile of *R*2′-OH in methylcobalamin [45–47]. The exchange rates k_{ex} are given in s^{-1}; solid curves were drawn using Eq. (9). NMR solutions: 10 mM solutions, sample size 0.7 cm^3, buffered with 8 mM, 10 mM, 15 mM, 40 mM, 70 mM and 100 mM phosphate buffer solutions, *pH* 5.0, as well as 10 mM solutions, sample size 0.7 cm^3, buffered with 100 mM phosphate buffer in the *pH* range from 4.5 to 7.6; 26°C. Intermolecular exchange rates (k_{ex}) were determined from selective T_2-measurements based on the equation $1/T_2 = 1/T_2(\text{dipolar}) + k_{ex}$. Selective RF pulses: excitation: 30 ms 270° *Gaussian* excitation pulse [53]; inversion: 50 ms G3 *Gaussian* cascade [54]. The T_2-values were corrected for the dipolar contribution to the linewidth $1/T_2$ (dipolar) and exchange contributions due to phosphate catalyzed intermolecular exchange. The dipolar contribution to the linewidth was determined to be 2.0 Hz by extrapolating the T_2-value to zero concentration of both catalysts, (hydrogen phosphate (HPO_4^{2-}) and hydroxyl ion (OH^-)

establishment of the internal equilibrium is much faster than the external exchange processes. From analysis of the exchange rate *vs. pH* profile according to Eq. (10) and using Eq. (7) for calculation of the intrinsic exchange rate, the equilibrium constant K_{eq} for reversible hydrogen bond formation of the *R*2′-OH hydrogen was calculated to $K_{eq} = 88$. From the value of K_{eq} determined this way, the *Gibbs* free energy of protection (ΔG_{prot}) was then determined from the expression $\Delta G_{prot} = -RT\ln K_{eq}$, yielding a value for ΔG_{prot} of $-11.3\,kJ \cdot mol^{-1}$. The *Gibbs* free energy of protection corresponds to the difference between the *Gibbs* free energy of a state (''protected state'') in which the *R*2′-OH proton acts as a hydrogen bond donor to the bound water molecule, and an ''unprotected'' state in which the protecting hydrogen bond is broken and in which the *R*2′-OH proton forms a weaker hydrogen bond to a bulk water acceptor molecule. In this ''unprotected'' state, the *R*2′-OH proton is accessible to the exchange catalyst (*e.g.* OH^-) and the bulk water. Our result for the free energy of protection ($\Delta G_{prot} = -11.3\,kJ \cdot mol^{-1}$) of a ribose *R*2′-OH significantly differs from a value previously obtained in wet *DMSO* solutions [109]. For cyclic nucleotide monophosphates, free energies of protection by an assumed water molecule were obtained there whose magnitudes were considerably smaller ($-6.3\,kJ \cdot mol^{-1}$) than the values obtained by us. This difference emphasizes the importance of the solvent as H-bond partner with respect to the strength of the H-bond. Our value of $\Delta G_{prot} = -11.3\,kJ \cdot mol^{-1}$ compares favorably with the recently determined effect of a point mutation of a single nucleotide to a 2′-deoxynucleotide upon the binding of *RNA* substrate in the catalytic core of the *Tetrahymena* ribozyme [110]: the major contributor to the increased stability of the *RNA* complex (compared to that of the mutant) could be traced back to the *R*2′-OH of a critical nucleotide residue and N1 of an adenosine. The elimination of a specific *R*2′-OH hydrogen bond donor by substituting a ribonucleotide by a 2-deoxyribonucleotide leads to a 33-fold increase in the dissociation constant (K_d) of oligonucleotide binding to *Tetrahymena* ribozyme, representing a difference in free energy ($\Delta\Delta G$) of $9.2\,kJ \cdot mol^{-1}$. This value was suggested to correlate closely with the free energy of the H-bond between a *R*2′-OH and the adenosine N1. Information about the energetics of hydrogen bonding interactions in biomolecules in aqueous solution, although highly desirable [111], is scarce [3, 4]. Deletions (*e.g.* by point mutations) of hydrogen bonding groups in proteins [112] and nucleic acids [113], often where found to lead to very small changes in the thermodynamic stability, presumably by replacing a direct hydrogen bond by a water-mediated hydrogen bond, or by changing one or both hydrogen bonding partners. Such compensating structural effects make it thus very difficult to determine accurately the strength of individual hydrogen bonds simply by evaluating the free energy difference caused by the deletion of a particular hydogen bond. Thus, dynamic NMR studies provide unique experimental access to hydrogen bonding energies in aqueous solution.

Conclusion

Increases in our knowledge of and our ability to experimentally measure hydrogen bond induced changes in H/D isotope fractionation, proton chemical shift anisotropy (CSA), and intermolecular exchange processes with bulk water

molecules provide a rich avenue to analyze systems in aqueous solution and acquire information by NMR spectroscopy not generally accessible by other means. Recent work has shown how detailed information on hydrogen bonded protons can be obtained by these solution NMR approaches. It is anticipated that additional theoretical work will provide physical insight into the correlations between H/D isotope fractionation, proton chemical shift anisotropy, and hydrogen bond energies and that these NMR approaches will advance our current understanding of hydrogen bonding and its impact on the structural propensities of molecules containing exchange labile hydrogens.

Acknowledgements

This work was supported by the *Austrian National Science Foundation* FWF (Project No. P10816-GEN and P11600-GEN). We are grateful to *Hoffmann-La Roche*, Basel, Switzerland, for a generous gift of vitamin B_{12}.

References

[1] Early consideration of a ''hydrogen bond'': a) Moore TS, Winwill TF (1912) J Chem Soc **101**: 1635; b) Latimer WM, Rodenbush WH (1920) J Am Chem Soc **42**: 1419
[2] Pauling L, Corey RB, Branson HR (1951) Proc Natl Acad Sci **37**: 205; Pauling L (1960) The Nature of the Chemical Bond, 3rd edn. Cornell University Press, New York
[3] Hibbert F, Emsley J (1990) Adv Phys Org Chem **26**: 255
[4] Jeffrey GA, Saenger W (1994) Hydrogen Bonding in Biological Structures, 2nd edn. Springer, Berlin Heidelberg
[5] Bernstein J, Etter MC, Leiserowitz L (1994) In: Bürgi H-B, Dunitz JD (eds) Structure Correlation, vol 2. VCH, Weinheim, p 431
[6] Lehn JM (1995) In: Supramolecular Chemistry: Concepts and Perspectives. VCH, Weinheim
[7] Lehn JM (1993) Science **260**: 1762
[8] Curtiss LA, Frurip DJ, Blander M (1979) J Chem Phys **71**: 2703
[9] Bürgi T, Droz T, Leutwyler S (1995) Chem Phys Lett **246**: 291
[10] Frey PA, Whitt SA, Tobin JB (1994) Science **264**: 1927
[11] Shan S, Loh S, Herschlag D (1996) Science **272:** 97
[12] Kato Y, Toledo LM, Rebek J Jr (1996) J Am Chem Soc **118**: 8575
[13] Schwarz B, Drueckhammer DG (1995) J Am Chem Soc **117:** 11902
[14] Ditchfield R (1976) J Chem Phys **65**: 3123
[15] McMichael Rohlfing C, Allen LC, Ditchfield R (1983) J Chem Phys **79**: 4958
[16] Berglund B, Vaughan RW (1980) J Chem Phys **73**: 2037
[17] Reimer JA, Vaughan RW (1980) J Magn Reson **41**: 483
[18] Gerald R, Bernhard T, Haeberlen U, Rendell J, Opella SJ (1993) J Am Chem Soc **115**: 777
[19] Wu CH, Ramamoorthy A, Gierasch LM, Opella SJ (1995) J Am Chem Soc **117**: 6148
[20] Ramamoorthy A, Wu CH, Opella SJ (1997) J Am Chem Soc **119**: 10479
[21] Llinás M, Wilson DM, Klein MP (1977) J Am Chem Soc **99**: 6846
[22] Llinás M, Horsley WJ, Klein MP (1976) J Am Chem Soc **98**: 7554
[23] Llinás M, Klein MP (1975) J Am Chem Soc **97**: 4731
[24] Facelli JC, Pugmire RJ, Grant DM (1996) J Am Chem Soc **118**: 5488
[25] Smirnov SN, Golubev NS, Denisov GS, Benedict H, Schah-Mohammedi P, Limbach HH (1996) J Am Chem Soc **118**: 4094
[26] Ash EL, Sudmeier JL, De Fabo EC, Bachovchin WW (1997) Science **278**: 1128
[27] Fujiwara FY, Martin JS (1974) J Am Chem Soc **96**: 7625

[28] Juranic N, Likic VA, Prendergas FG, Macura S (1996), J Am Chem Soc **118**: 7859
[29] Abragam A (1986) Principles of Nuclear Magnetism, Oxford Univ Press, Oxford
[30] Schmidt-Rohr K, Spiess HW (1994) Multidimensional Solid-State NMR and Polymers, Academic Press, London
[31] Shimizu H (1964) J Chem Phys **40**: 3357
[32] Mackor EL, MacLean C (1966) J Chem Phys **44**: 64
[33] Goldman M (1984) J Magn Reson **60**: 437
[34] Guéron M, Leroy JL, Griffey RH (1983) J Am Chem Soc **105**: 7262
[35] Burghardt I, Konrat R, Bodenhausen G (1992) Mol Phys **75**: 467
[36] Dalvit C, Bodenhausen G (1989) Chem Phys Lett **161**: 554
[37] Konrat R, Nutz K, Kalcher J, Sterk H (1994) J Phys Chem **98**: 7488
[38] McConnell HM (1956) J Chem Phys **25**: 709
[39] Konrat R, Sterk H (1993) Chem Phys Lett **203**: 75
[40] Reif B, Hennig M, Griesinger C (1997) Science **276**: 1230
[41] Yang D, Konrat R, Kay LE (1997) J Am Chem Soc **119**: 11938
[42] Tjandra N, Bax A (1997) J Am Chem Soc **119**: 8076
[43] Tessari M, Mulder FAA, Boelens R, Vuister GW (1997) J Magn Reson **127**: 128
[44] Tessari M, Vis H, Boelens R, Kaptein R, Vuister GW (1997) J Am Chem Soc **119**: 8985
[45] Tollinger M, Konrat R, Kräutler B (1997) J Mol Catal **116**: 147
[46] Konrat R, Tollinger M, Kräutler B (1998) In: Kräutler B, Arignoi D, Golding BT (eds) Vitamin B_{12} and B_{12}-Proteins. Wiley-VCH, Weinheim
[47] Tollinger M, Konrat R, Kräutler B (manuscript in preparation)
[48] Rossi M, Glusker JP, Randaccio L, Summers MF, Toscano PJ, Marzilli LG (1985) J Am Chem Soc **107**: 1729
[49] Liepinsh E, Otting G, Wüthrich K (1992) J Biomol NMR **2**: 447
[50] Leroy JL, Broseta D, Gueron M (1985) J Mol Biol **184**: 165
[51] Poppe L, van Halbeek H (1991) J Am Chem Soc **113**: 363
[52] (a) Carr HY, Purcell EM (1954) Phys Rev **94**: 630; (b) Meiboom S, Gill G (1958) Rev Sci Instrum **29**: 688
[53] Emsley L, Bodenhausen G (1989) J Magn Reson **82**: 211
[54] Emsley L, Bodenhausen G (1990) Chem Phys Lett **165**: 469
[55] Rhim WK, Burum DP, Elleman DD (1979) J Chem Phys **71**: 3139
[56] Ryan LM, Wilson RC, Gerstein BC (1977) Chem Phys Lett **52**: 341
[57] Pines A, Ruben DJ, Vega S, Mehring M (1976) Phys Rev Lett **36**: 110
[58] Hinton JF, Bennett DL (1985) Chem Phys Lett **116**: 292
[59] Schowen KB, Schowen RL (1982) Meth Enzym **87**: 551
[60] Hvidt A, Nielsen SO (1966) Adv Prot Chem **21**: 287
[61] Kresge AJ (1964) Pure Appl Chem **8**: 243
[62] Jarret RM, Saunders M (1985) J Am Chem Soc **107**: 2648
[63] Jarret RM, Saunders M (1986) J Am Chem Soc **108**: 7549
[64] Cleland WW (1980) Meth Enzymol **64**: 104
[65] Krevoy MM, Liang TM (1980) J Am Chem Soc **102**: 3315
[66] Cleland WW (1992) Biochemistry **31**: 317
[67] Weiss PM, Cook PF, Hermes JD, Cleland WW (1987) Biochemistry **26**: 7378
[68] Weiss PM, Boerner RJ, Cleland WW (1987) J Am Chem Soc **109**: 7201
[69] Loh SN, Markley JL (1993) In: Angletti R (ed) Techniques in Protein Chemistry IV. Academic Press, San Diego, p 517
[70] Loh SN, Markley JL (1994) Biochemistry **33**: 1029
[71] LiWang AC, Bax A (1996) J Am Chem Soc **118**: 12864
[72] Bothner-By AA, Stephens RL, Warren CD, Jeanloz RW (1985) J Am Chem Soc **106**: 811
[73] Piotto M, Saudek V, Sklenár V (1992) J Biomol NMR **2**: 661

[74] Van de Ven FJM, Hansen HGJM, Gräslund A, Hilbers CW (1988) J Magn Reson **79**: 221
[75] Davis DG, Bax A (1985) J Am Chem Soc **107**: 2820
[76] Englander SW, Kallenbach NR (1984) Quart Rev Biophys **16**: 521
[77] Bai Y, Milne JS, Mayne L, Englander SW (1993) Proteins **17**: 75
[78] Connelly GP, Bai Y, Jeng MF, Englander SW (1993) Proteins **17**: 87
[79] Englander JJ, Rogero JR, Englander SW (1985) Anal Biochem **147**: 234
[80] Eigen M (1964) Angew Chem **3**: 1
[81] Haslam JL, Eyring EM (1967) J Phys Chem **71**: 4470
[82] Rose MC, Stuehr J (1968) J Am Chem Soc **90**: 7205
[83] Linderstrøm-Lang KU (1955) In: Symposium on Peptide Chemistry. Chem Soc Spec Publ **2**: 1
[84] Linderstrøm-Lang KU (1958) In: Neuberger A (ed) Symposium on Protein Structure. Methuen London
[85] Woodward CK, Simon I, Tuchsen E (1982) Mol Cell Biochem **48**: 135
[86] Berger A, Linderstrøm-Lang KU (1957) Archs Biochem Biophys **69**: 106
[87] Wagner G (1983) Quart Rev Biophys **16**: 1
[88] Barksdale AD, Rosenberg A (1976) Meth Biochem Anal **28**: 1
[89] Zhang YP, Lewis RN, Henry GD, Sykes BD, Hodges RS, McElhaney RN (1995) Biochemistry **34**: 2348
[90] De Jongh HH, Goormaghtigh E, Ruysschaert JM (1995) Biochemistry **34**: 172
[91] Hildebrandt P, Vanhecke F, Heibel G, Mauk AG (1993) Biochemistry **32**: 14158
[92] Englander JJ, Calhoun DB, Englander SW (1979) Anal Biochem **92**: 517
[93] Kossiakoff AA (1982) Nature **296**: 713
[94] Pan Y, Briggs MS (1992) Biochemistry **31**: 11405
[95] Loh SN, Prehoda KE, Wang J, Markley JL (1993) Biochemistry **32**: 11022
[96] Rohl CA, Baldwin RL (1994) Biochemistry **33**: 7760
[97] Feng Y, Sligar FG, Wand AJ (1994) Nat Struct Biol **1**: 30
[98] Jeng M, Englander SW, Pardue K, Rogalskyi JS, McLendon G (1994) Nat Struct Biol **1**: 234
[99] Mayne L, Paterson Y, Cerasoli D, Englander SW (1992) Biochemistry **31**: 10678
[100] Ehrhardt MR, Urbauer JL, Wand AJ (1995) Biochemistry **34**: 2731
[101] Paterson Y, Englander SW, Roder H (1990) Science **249**: 755
[102] Forsén S, Hoffman RA (1963) J Chem Phys **40**: 1189
[103] Waelder S, Redfield AG (1977) Biopolymers **16**: 623
[104] Rosevaer PR, Fry DC, Mildvan AS (1985) J Magn Reson **61**: 102
[105] Krishna NR, Huang DH, Glickson JD, Rowan R, Walter R (1979) Biophys J **26**: 345
[106] Spera S, Bax A (1991) J Biomol NMR **1**: 155
[107] Sandström J (1982) In: Dynamic NMR Spectroscopy. Academic Press, New York
[108] Kratky C, Färber G, Gruber K, Wilson K, Dauter Z, Nolting HF, Konrat R, Kräutler B (1995) J Am Chem Soc **117**: 4654
[109] Bolton PH, Kearns DR (1979) J Am Chem Soc **101**: 479
[110] Pyle AM, Murphy FL, Cech TR (1992) Nature **358**: 123
[111] Fersht A (1985) In: Enzyme Structure and Mechanism. Freeman, New York
[112] Alber T, Sun DP, Wilson K, Wozniak JA, Cook SP, Matthews BW (1987) Nature **330**: 41
[113] Jucker FM, Heus HA, Yip PF, Moors EHM, Pardi A (1996) J Mol Biol **264**: 968

Received November 13, 1998. Accepted November 30, 1998